ACCEPTED MANUSCRIPT

From zinc-cyanide hybrid coordination polymers to hierarchical yolk-shell structures for high-performance and ultra-stable lithium-ion batteries

Haosen Fan[a, b, c], Hong Yu[b], Yufei Zhang[b], Jing Guo[a], Zhen Wang[a], Hao Wang[a], Xi Hao[a], Ning Zhao[a*], Hongbo Geng[b], Zhengfei Dai[b], Qingyu Yan[b, c*] and Jian Xu[a*]

[a] *Beijing National Laboratory for Molecular Sciences, Institute of Chemistry, Chinese Academy of Sciences, Beijing, 100190, P.R. China*

[b] *School of Materials Science and Engineering, Nanyang Technological University, 639798, Singapore*

[c] *Energy Research Institute@NTU, Nanyang Technological University, Research Techno Plaza, 637553, Singapore*

E-mail: zhaoning@iccas.ac.cn;

alexyan@ntu.edu.sg;

jxu@iccas.ac.cn

Accepted manuscript

Abstract:

Uniform zinc-cyanide hybrid coordination polymer microspheres were successfully synthesized by a coprecipitation method. Then hierarchical yolk-shell structured and carbon coated ZnO microspheres (YC-ZnO) composed of ZnO@C nanocrystals were prepared by consecutive post annealing processes of these microspheres in argon and air atmosphere. Such micro-nano porous structures have the advantages of large specific surface area, good charge transport kinetics, and large cavity to accommodate the volume change and maintain the mechanical integrity of the electrode material. When evaluated as anode materials of lithium ion batteries, these ZnO yolk-shell spheres exhibited excellent battery performance with a high rate capacity and ultra-stable cycling stability.

Graphical abstract

ACCEPTED MANUSCRIPT

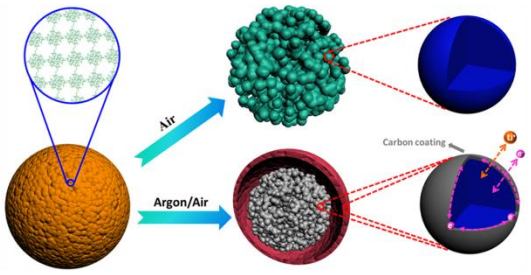

Keywords: coordination polymers; batteries; ultra-stable; yolk-shell; ZnO@C nanocrystal;

1. Introduction

Lithium-ion batteries (LIBs) are one kind of energy storage devices based on the chemical reversible redox reactions between lithium ions and positive/negative electrode materials [1-4]. To meet the ever-growing demands of various consumer electronic devices, high-performance electrode materials with large capacities, long cycle life and low cost are highly demanded [5-7]. However, bulk materials often suffer from serious capacity degradation during the discharge and charge process because of the slow charge diffusion process and pulverization of the active materials [8]. On the other side, although nanomaterials exhibit advantages of large specific surface area and short Li diffusion paths, they are often suffered from aggregation, low packing density and high processing cost. Recently, micro-nano secondary structure materials have attracted great interests as electrode materials, due to their dual advantages: the micro characteristics allow to achieve high packing density and the nano characteristics facilitate the Li^+ ion diffusion.

As a typical transition metal oxide, ZnO has attracted much attention as an alternative anode due to the high theoretical lithium storage capacity (987 mAh g^{-1}), low cost, easy to prepare and chemically stable. Most importantly, ZnO-based electrode materials have higher lithium-ion diffusion coefficients compared to other transition metal oxides [9-11]. However, the inherent poor electrical conductivity and large volume expansion upon cycling cause the low reversible capacity, severe capacity fading (usually 200 mAh g^{-1} in just a few cycles), and poor rate performances. Therefore, a lot of efforts have been devoted to overcome the above mentioned issues. Modify the material by incorporating composite, doping or coating with carbon layer are commonly used approaches [12-14]. Besides, combining ZnO with other metal oxides to form heterostructures [15-18] have been demonstrated to effectively improve the Li ion storage property [19, 20]. However, rational design and controllable preparation of micro-nano structure ZnO electrode materials, especially porous yolk-shell structure, is challenging.

Accepted manuscript

ACCEPTED MANUSCRIPT

The porous yolk-shell structure constructed by nanometer-sized subunits can provide short Li diffusion length. The porous shells can allow effective interaction between the electrode materials and electrolyte by providing accessible channels. Besides, the large space between yolk and shell is useful to accommodate the volume change and keep the integrity of the yolk-shell structure during the charge/discharge process.

Herein, we present a facile copreciptation method to prepare Zn-based coordination polymer (ZnCP) microspheres assembled from nanoparticles. After annealing processes in argon and air, hierarchical yolk-shell structured and carbon coated ZnO microspheres (noted as YC-ZnO) built up by ZnO@C nanocrystals were obtained. The YC-ZnO exhibits porous structure with the diameter of about 1 μm. The shell thickness is about 80 nm and the yolk size is about 600 nm. Both the yolk and shell are composed of ZnO nanocrystals (size about 30 nm) and carbon. When evaluated as anode materials for LIB, these YC-ZnO shows high capacities (1169 mAh g^{-1}), excellent rate capablities (a discharge capacity of 289.6 mA g^{-1} at the current density of 10 A g^{-1}), and stable cycling performance (96.9 % capacitiy retention after 5000 cycles).

2. Experimental Section

2.1 Preparation of monodispersed $Zn[Zn(CN)_4]•xH_2O$ microspheres (ZnCP)

A aqueous co-precipitation method was used to synthesize ZnCP microspheres: firstly, 0.4 g PVP and 0.2 mmol $ZnCl_2·6H_2O$ were added into 20 mL deionized water and completely dissolve. Then, 0.2 mmol $K_2Zn(CN)_4$ was dissolved into another 20 mL deionized water to form clear solution. The two solutions were mixed together and stirred for 30 min. The mixed solutions were kept stationary state at room temperature for 24 hours. The obtained white precipitation was filtered and washed for several times and subsequently dried at 60 °C for 24h in a vacuum drying oven.

To prepare ZnO, 50 mg ZnCP microspheres were calcinated in a corundum crucible at 500 °C for 3 h in air with a heating rate of 2 °C·min^{-1}. To prepare YC-ZnO, 50 mg ZnCP microspheres were calcinated at 500 °C for 3 h in argon (2 °C·min^{-1}). After cool down to room temperature, the sample then were calcinated at 300 °C for 3 h in air (2 °C·min^{-1}).

2.2 Materials characterization

X-ray diffraction (XRD) patterns were tested on a Micscience M-18XHF using CuKa radiation. Morphology and structure was studied by scanning electron microscope (SEM, 7500F) and transmission electron microscope (TEM, JEM-2100F). Particle size analysis of the ZnCP suspension

Accepted manuscript

ACCEPTED MANUSCRIPT

was performed on a Zetasizer (Malvern, Nano-ZS). The X-ray photoelectron spectroscopy spectrum (XPS) was conducted on a Thermo VGESCALAB250 X-ray photoelectron spectrometer. The nitrogen adsorption/desorption isotherms were obtained at 77K using a Quantachrome Autosorb-1CVP analyzer.

2.3 Electrochemical measurements

The batteries properties were measured using CR2032 coin cells assembled in an argon-filled glove-box. The anodes slurry were fabricated by mixing 70 wt% electrode materials, 20 wt% acetylene black and 10 wt% poly(vinyldifluoride) (PVDF) in N-methyl-2-pyrrolidone (NMP) solvent. Then the slurry was coated on copper foils to obtain the working electrodes and dry at 70 °C overnight. The electrolyte solution was 1 M $LiPF_6$ in ethylene carbonate (EC)/diethyl carbonate (DEC) (1:1, w/w) and lithium foil serves as counter electrode. After assembling the cells in an argon-filled glove box, galvanostatic discharge-charge tests were performed using a NEWARE battery tester at a voltage window of 0.001-3.0 V and cyclic voltammetry (CV) was performed with an electrochemical workstation (Solarton) at the scan rate from 0.1 to 2 mV s^{-1}.

3. Results and Discussions

Uniform sized ZnCP microspheres have been successfully synthesized based on a precipitation reaction, as shown in Fig. 1a. From the SEM images (Fig. 1b-c), the microspheres show granular topography. Meanwhile, cross-section image of a broken ZnCP microsphere reveals that the microsphere is constructed by the aggregation of ZnCP nanocrystals (Fig. 1d). TEM image (Fig. 1e) clearly exhibits the uniform spherical shape. The high-resolution TEM (HRTEM) image of the edge of the microsphere (Fig. 1f) demonstrates that it is well crystalline with the lattice spacing $d_{(110)}$ = 0.42 nm. The uniformity of ZnCP microspheres was further summarized by particle size distribution (Fig. 1g), which shows a narrow distribution with an average diameter of about 1.2 μm. The X-ray diffraction (XRD) spectrum (Fig. 1h) is in agreement with a body center cubic (*bcc*) structure of $Zn(CN)_2$ (JCPDS card no. 06-0175, space group *P-43m*, a=b=c=5.905 Å, α=β=γ=90°). In the molecular structure of $Zn(CN)_2$ (Fig. 1i), each Zn atom is surrounded by four neighboring cyano groups forming a Zn-centered tetrahedron [21, 22]. Hence, a ZnCP unit is composed of two interconnected $Zn(CN)_2$ molecules via linear Zn-CN-Zn linkages of two tetrahedral Zn^{2+} cations (dashed box).

Accepted manuscript

ACCEPTED MANUSCRIPT

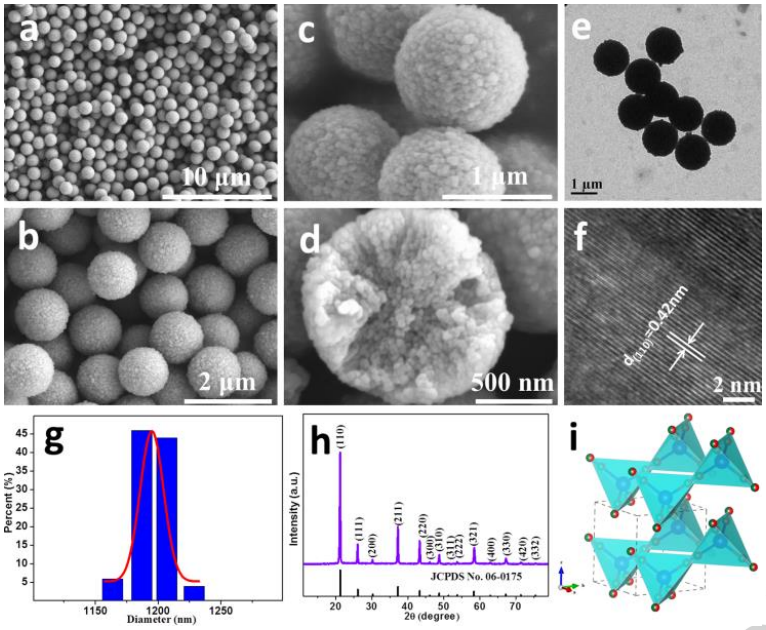

Fig. 1. (a, b, c and d) SEM images of the synthesized ZnCP precursor microspheres. (e and f) TEM images of as-prepared monodispersed ZnCP microspheres. (g) Size distribution of ZnCP microspheres. (h) XRD pattern of ZnCP microspheres. (i) Spatial structure of ZnCP microspheres.

Fig. S1a (Supporting information) shows the X-ray diffraction (XRD) patterns of as-prepared ZnO and YC-ZnO, which confirm that both the pruducts were wurtzite-type ZnO with hexagonal close-packed (*hcp*) structures (JCPDS card no. 36-1451). There are no detectable peaks from impurity phase. Fig. S1b (Supporting information) illustrates the spatial structure of *hcp* ZnO with a *P63mc* space group, a=b=3.25 Å, c=5.21 Å, α=β=90°, γ=120°. The SEM images of as-prepared pure ZnO and YC-ZnO were shown in Fig. 2. Annealing the ZnCP in air results in porous ZnO microspheres with an average diamenter of about 1 μm (Fig. 2a). The magnified SEM images (Fig. 2b and c) show the ZnO microspheres are composed of many ZnO nanocrystals with the size of about one hundred nanometers, randomly aggregated together to form the sphere structure. TEM examination (Fig. 2d) further exhibites the aggregated ZnO nanocrystals with porous structures in a single microsphere. When the ZnCP micropheres were annealed in argon and then in air, YC-ZnO were obtained (Fig. 2e). The average diameter is on the order of 1 μm (Fig. 2f). Some broken microspheres clearly reveal the inner core (the diameter of about 600 nm), outer shell (the thickness of about 70 nm) as well as the interstitial void space. From the magnified SEM micrograph of a single microsphere (Fig. 2g), it can be observed that the core is porous and built up by the randomly aggregated nanocrystals with an average size of about 30 nm, however, the coated shell is complete and is consisted of compacted nanocrysatls. The package-effective shell is conducive to maintain the structure stability. TEM image

Accepted manuscript

(Fig. 2h) further clearly demonstrates the yolk-shell structures are highly porous with an obvious gap between the inner core and the outer shell.

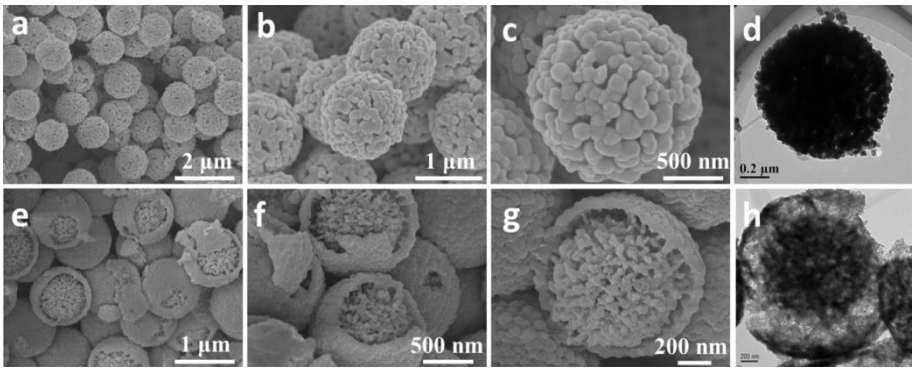

Fig. 2. SEM and TEM images of ZnO microspheres (a-d) and yolk-shell structured YC-ZnO (e-h).

High-resolution TEM (HRTEM) and High Angle Annular Dark Field-Scanning Transmission Electron Microscopy (HAADF-STEM) investigations were further used to confirm the morphology of YC-ZnO. It is clearly that the yolk shell structures are uniform and composed of numerous ZnO@C nanocrystals (Fig. 3a-b). The selected area image of the yolk (Fig. 3c) and the shell (Fig. 3d) clearly show the porous structure with numerous nano-scaled pores. Similar to the SEM result, the yolk demonstrates the more porous and loose structure than that of the shell. The ZnO nanocrystals are wrapped by the continuous carbon layers with a thickness of about 3-5 nm, forming ZnO@C structure (Fig. 3e and 3f). The carbon layer can form an effective conducting network for bridging each individual ZnO nanocrystals. The HRTEM image of the yolk part (Fig. 3 g) shows the obvious lattice fringes with the spacing of 0.28, 0.26 and 0.25 nm, corresponding to the distance between (100), (002), and (101) planes of ZnO, respectively. HAADF-STEM image (Fig. 3 h) reveals that the YC-ZnO are indeed composed of Zn, O, C and N elements, which homogenously distribute to form an entire yolk-shell structure.

Accepted manuscript

ACCEPTED MANUSCRIPT

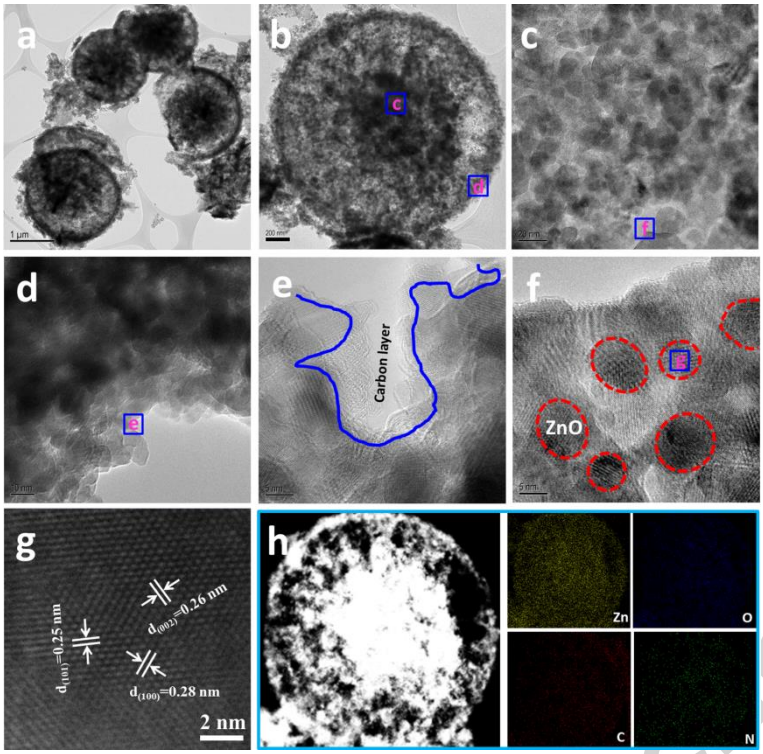

Fig. 3. (a-b) TEM images of YC-ZnO. (c-d) Regional TEM images of the porous yolk and shell. (e-f) TEM images of the ZnO nanocrystal coated with carbon layer. (g) HRTEM image of lattice structure of ZnO nanocrystal. (h) HAADF-STEM and elemental mapping of a single YC-ZnO.

According to the SEM and TEM characterizations discussed above, the annealing conditions have a profound influence on the morphology of the product when using ZnCP microspheres as the precursor. A possible formation mechanism is schematically shown in Fig. 4. When annealed the ZnCP in argon atmosphere fisrt and then in air, yolk-shell structures composed by ZnO@C nanocrystals were obtained. In the initial stage, the surface nanoparticles decompose to form a dense ZnO shell (Fig. S2, Supporting information). Then inner nanoparticles gradually decompose. Owing to the temperature gradient between the suface and the inner of microsphere, it leads to the different decomposition rates and the shrinkage of the microspheres. As a result, yolk-shell structures are generated. Meanwhile, porous structure was obtained due to the decomposition of cyano groups in the microspheres. However, when annealed in air, the oxidative decomposition of the ZnCP microspheres can start uniformly inside the sphere as the structures are relatively porous, which results in polycrystalline ZnO microspheres.

Accepted manuscript

ACCEPTED MANUSCRIPT

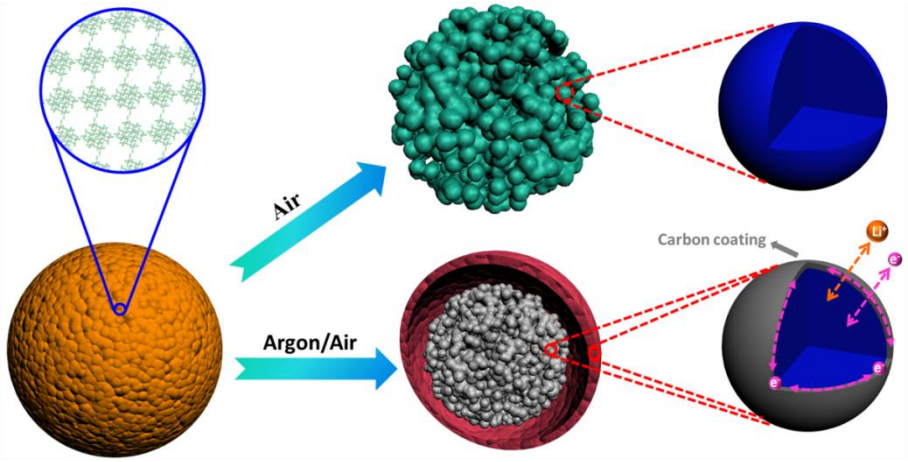

Fig. 4. Schematic illustrating the synthesis of hierarchical yolk-shell structure assembled from porous ZnO@C nanocrystals.

Nitrogen absoprtion and desorption curve is shown in Fig. 5a. The calculated Brunauer-Emmett-Teller (BET) specific surface area of YC-ZnO is 102.237 m^2 g^{-1}. The pore size distribution plots (inset in Fig. 5a) further reveals that the mesoporous structures, with the pore size of 2-8 nm, are predominant in the as-prepared materials. The Raman spectrum of YC-ZnO (Fig. 5b) indicates that the graphitization degree is 0.967, which is calculated based on the intensity ratio of the D band to the G band (I_D/I_G). Such high degree of graphitization may lead to a good electrical conductivity [23]. X-ray photoelectron spectroscopy (XPS) was used to determin the Elemental composition. The N1s peak shown in Fig. 5c corresponds to nitrogen atoms in C=N bonds (398.3 eV) and C-N bonds (400.5 eV), implying the formation of pyridine-like N (C=N bond) and graphite-like N (C-N bond) in the carbon of YC-ZnO due to the decomposition of cyano groups [24]. The concentration of nitrogen was confirmed to be 3.4 wt% in carbon framework. Fig. 5d shows the XPS spectrum of Zn $2p_{3/2}$ and $2p_{1/2}$ at aroud 1021.8 and 1044.8 eV. This in good agreement with the standard table for elements signals, indicating the successful synthesis of ZnO nanocrystals.

Accepted manuscript

ACCEPTED MANUSCRIPT

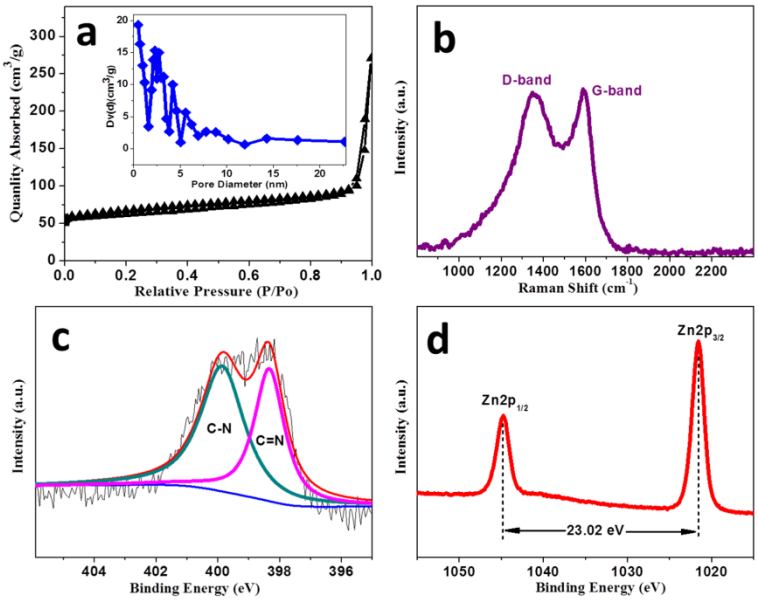

Fig. 5. (a) Nitrogen adsorption/desorption isotherms and pore size distribution (insets) of YC-ZnO. (b) Raman spectrum of of YC-ZnO. (c) N1s and (d) Zn2p XPS spectra of YC-ZnO.

The electrochemical properties of the obtained ZnO and YC-ZnO were investigated by using cyclic voltammetry in the potential range of 0.001-3 V. Fig. 6a shows the initial 5 cycles of YC-ZnO electrode at a scan rate of 0.1 mV s^{-1}. In the first cathodic scan, the strong peak at about 0.37 V is related to the reduction of ZnO to Zn, the formation of Li_2O, the formation of LiZn alloy, and the formation of solid electrolyte interphase (SEI). In the subsequent cathodic scans, the major peak splits into two peaks concentrated at 0.7 and 0.1 V, corresponding to the reduction of ZnO to Zn and the alloy formation of lithium and zinc [25], respectively. From the first anodic scan onward, there are three small oxidation peaks between 0.2 and 0.7 V, which can be assigned to the multistep dealloying reactions of LiZn→ Li_2Zn_3→$LiZn_2$→Li_2Zn_5→LiZn and the decomposition of SEI layer [26, 27]. Besides, a smooth peak at around 1.5 V may be ascribed to the reversible redox conversion reaction between Zn and Li_2O to form ZnO [28]. In the subsequent cycles, both cathodic and anodic curves peaks overlap well with each other, demonstrating the improved reversibility of the electrochemical reactions. As a comparison, the CV curves of ZnO solid spheres show poor stability, which display the obvious decay of current density along with the increase of cycle numbers (Fig. S3, Supporting information). Fig. 6b shows the CV curves of YC-ZnO electrode at various scan rates ranging from 0.1 mV s^{-1} to 2.0 mV s^{-1}. The intensity of the cathodic and anodic peaks increases with scan rates. Theoretically, the ratio between the peak area and the scan rate is the capacity of the electrode, which is considered to be constant. The

Accepted manuscript

ACCEPTED MANUSCRIPT

dependence of the cathodic and anodic peak currents on the square root of the scan rate ($v^{1/2}$) is presented in Fig. 6c and d. It can be clearly seen that both cathodic and anodic peaks show a linear relationship with $v^{1/2}$. The classical Randles-Sevchik equation (Equation 1) for a semi-infinite diffusion is used to fit the linear curves [29]:

$$i_p = (2.69\times10^5)n^{3/2}SD^{1/2}Cv^{1/2} \quad (1)$$

in which i_p is the peak current (A), n is the charge-transfer number, S is the electrode area, D is the diffusion coefficient of Li^+ ($cm^2\ s^{-1}$), C is the concentration of lithium ions, and v is the potential scan rate ($V\ s^{-1}$). Since all the electrodes were prepared and tested from the same procedure, the Randles-Sevchik equation can be simplified as:

$$i_p = AD^{1/2}v^{1/2} \quad (2)$$

where A is regarded as a constant for the LIBs, and $AD^{1/2}$ is defined as the apparent diffusion coefficient of Li^+ in the cells. According to the fitting results, the YC-ZnO shows the diffusion coefficients of Li^+ with 0.70 for positive peaks and 3.63 for negative peaks, respectively, which are much higher than that of solid ZnO spheres (0.48 and 0.53). The enhanced Li^+ diffusion behavior would improve the lithiation/delithiation reaction kinetics.

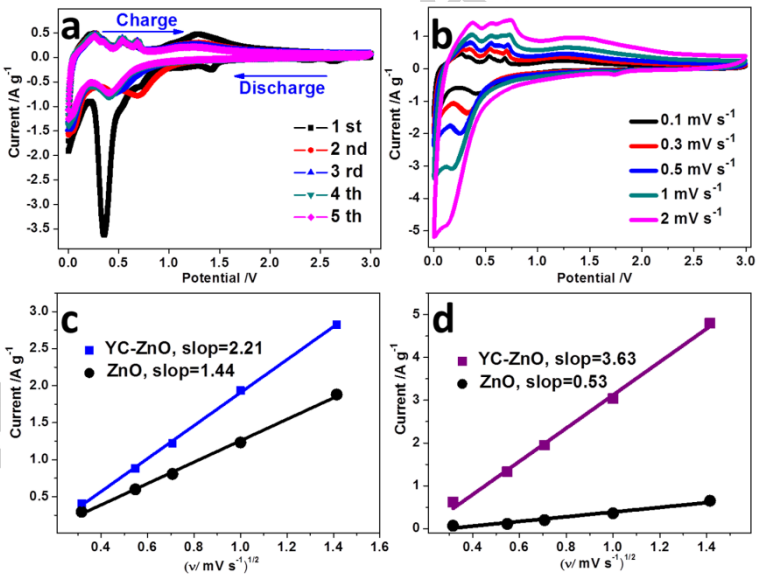

Fig. 6. (a) CV curves of YC-ZnO electrode at a scan rate of 0.1 mV s^{-1} within a potential range of 0.001 to 3.0 V; (b) CV curves of YC-ZnO electrode at various scan rates from 0.1 mV s^{-1} to 2.0 mV s^{-1}; (c) The linear relationship of the cathodic peak current (i_p) and the square root of scan rate ($v^{1/2}$) for ZnO and YC-ZnO; (d) The linear relationship of the anodic peak current (i_p) and the square root of scan rate ($v^{1/2}$) for ZnO and YC-ZnO.

ACCEPTED MANUSCRIPT

The galvanostatic charge/discharge curves of the ZnO and YC-ZnO batteries at 0.1 A g^{-1} are shown in Fig. 7a. It shows initial discharge capacities of 1501 mAh g^{-1} with the coulombic efficiency of 77.8%, which is higher than that of solid ZnO spheres (1208mAh g^{-1} and 72.4%). From the 10th cycle onwards, the curves almost overlap each other, implying the good electrochemically reversibility (Fig. 7b). Fig. 7c and 7d exhibits the rate capability of YC-ZnO electrode. The discharge capacities are 1045.2, 789.9, 632.4 573.0 and 485.7 mAh g^{-1} at current densities of 0.1, 0.2, 0.5, 1 and 2 A g^{-1}, respectively. At the relatively high current densities of 5 and 10 A g^{-1}, the capacities are maintained to be 372.5 and 289.6 mA g^{-1}, respectively. In contrast, the solid ZnO spheres depict a specific capcaity of only 41 mAh g^{-1} at a current denisty of 10 A g^{-1} (Fig. S4, Supporting information). Fig. 7e shows the cycling performance of the solid ZnO spheres and YC-ZnO. During the 50th cycle, the YC-ZnO electrode shows the discharge capaciy of 818 mAh g^{-1} while the solid ZnO spheres give only 510 mAh g^{-1}. Nyquist plots reveal a smaller charge transfer resistance (R_{ct}, the diameter of semicircle in the high-frequency region) of the YC-ZnO electrode in comparison with solid ZnO spheres (Fig. S5, Supporting information). The improved electrical conductivity is beneficial to achieve a faster charge transfer process. Fig. 7f summarizes comparison of the rate performance between the YC-ZnO and the reported state-of-the-art ZnO-based anodes, including ZnO QDs/graphene nanocomposites [30], ZnO/aligned graphene [31], ZnO/3D carbon framework [32], PEDOT-PSS coated ZnO/C nanorod [14], and other ZnO-based nanocomposites [11, 12, 33].

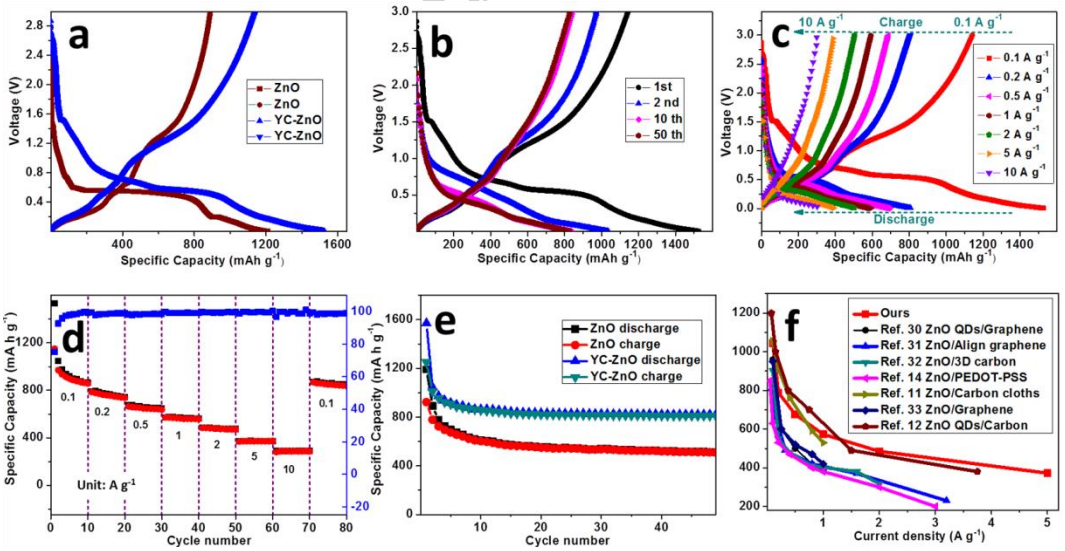

Fig. 7. (a) Charge/discharge curves of ZnO and YC-ZnO at the current density of 0.1 A g^{-1}. (b) Charge/discharge profiles at the 1st, 2nd, 10th, and 50th cycles of YC-ZnO electrode. (c) Charge/discharge curves of YC-ZnO electrode at various current densities. (d) Rate performance of YC-ZnO at various current densities from 0.1 to 10 A g^{-1}. (e) Cycling performance of ZnO and YC-ZnO electrodes at a current density of 0.1 A g^{-1}. (f) Comparison of the rate property of YC-ZnO to other reported ZnO based

electrodes.

The long-term cycling performance of YC-ZnO is shown in Fig. 8a. During the 300th cycle at the current density of 0.5 A g^{-1}, a discharge capacity of 659 mAh g^{-1} is retained. It should be noted that there are little increase of discharge/charge capacity upon cycling, which may be mainly attributed to the gradual activation process of the YC-ZnO electrode, as well as the reversible formation/dissolution of a polymer-like film around the electrode materials caused by the kinetically activated degradation of the electrolyte [34, 35]. In the following cycles at the current density of 2 A g^{-1}, YC-ZnO electrode also keep a stable discharge/charge capacity after 1000 cycles. Fig. 8b gives the cycling performance at high current desity of 10 A g^{-1}, further manifesting its superior cycling stability with 96.9 % retention rate after 5000 cycles.

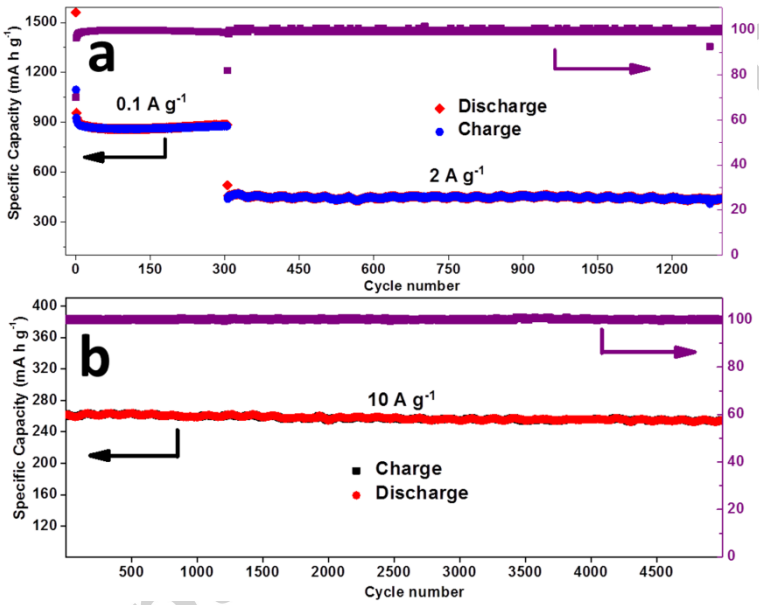

Fig. 8. (a) Long-term cycling performance of YC-ZnO electrode at the successive current density of 0.5 A g^{-1} and 2 A g^{-1}. (b) Cycling performance of YC-ZnO electrode at the current density of 10 A g^{-1} for 5000 cycles.

To further explore the advantage of YC-ZnO with super lithium ion storage property, we examined the SEM images (Fig. 9a-b) of the solid ZnO and YC-ZnO during 50th cycle at the current density of 0.1 A g^{-1}. YC-ZnO exhibit excellent structural stability by maintaining the yolk-shell structure while the solid ZnO microspheres have split into nanoparticles. The possible lithiation process of the solid ZnO and YC-ZnO electrodes was schematic presented in Fig. 9c. The solid ZnO spheres may be pulverized during charge/discharge process. But the morphological structure of YC-ZnO can keep unchange by providing the sufficient space between the yolk and the shell to accommondate the volume expansion. Hence, the YC-ZnO material possesses a significantly structural advantage over the solid ZnO: (1)

highly conductive carbon facilitates charge transfer into the inner of electrode material; (2) hollow space between the yolk and the shell can buffer the strain during repeated cycling to maintain the structural integrity; (3) the carbon layer serves as a self-supporting framework around ZnO nanocrystal, allowing ZnO nanocrystals to expand without cracking upon the lithiation prosess; (4) the yolk shell microspheres with micro-nano secondary structure allow to both achieve high packing density and facilitate the Li^+ ion diffusion.

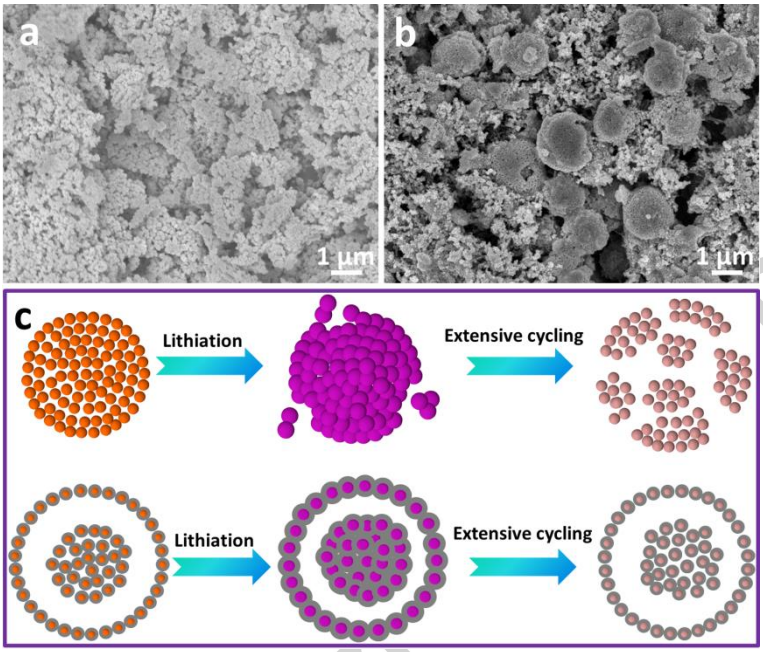

Fig. 9. (a) and (b) SEM images of solid ZnO and YC-ZnO sfter 50 cycles (c) Schematic illustration of the lithiation process in ZnO and YC-ZnO anodes.

4. Conclusion

In summary, a facile approach has been demonstrated to prepare yolk-shell YC-ZnO structures by thermally induced decomposition of a cyanide-bridged hybrid coordination polymer in argon and air atmosphere. The obtained YC-ZnO exhibited excellent rate capability and outstanding cycling stability due to its structural advantages, which are beneficial to improve the conductivity and buffer the volume expansion. Hence, the electrochemical properties and battery capacity are greatly enhanced in comparison to solid ZnO. By taking advantage of the unique reactivity of cyanide-bridged hybrid coordination polymer and the two step annealing method in this work, large-scale synthesis of unique functional nanomaterials with hollow and fascinating architectures could be expected for energy storage.

Accepted Manuscript

ACCEPTED MANUSCRIPT

Acknowledgements

Singapore MOE AcRF Tier 1 grants RG2/13, RG113/15, and Singapore A*STAR Pharos program SERC 1527200022 are gratefully acknowledged

References

[1] B. Scrosati, J. Hassoun and Y.-K. Sun, Energy & Environ. Sci. 4 (2011) 3287-3295.

[2] M. Yu, R. Li, M. Wu and G. Shi, Energy Storage Mater. 1 (2015) 51-73.

[3] P. G. Bruce, B. Scrosati and J. M. Tarascon, Angew. Chem. Int. Ed. 47 (2008) 2930-2946.

[4] Y. Zhong, M. Yang, X. Zhou, J. Wei and Z. Zhou, Part. Part. Syst. Charact. 32 (2015) 104-111.

[5] B. Sun, K. Huang, X. Qi, X. Wei and J. Zhong, Adv. Funct. Mater. 25 (2015) 5633-5639.

[6] H. Yu, H. Fan, B. Yadian, H. Tan, W. Liu, H. H. Hng, Y. Huang and Q. Yan, ACS Appl. Mater. Interfaces 7 (2015) 26751-26757.

[7] J. Chen, W. Song, H. Hou, Y. Zhang, M. Jing, X. Jia and X. Ji, Adv. Funct. Mater. 25 (2015) 6793-6801.

[8] Z. Y. Fan, J. Liang, W. Yu, S. J. Ding, S. D. Cheng, G. Yang, Y. L. Wang, Y. X. Xi, K. Xi, R. V. Kumar, Nano Energy 16 (2015) 152-162.

[9] B. N. Joshi, S. An, H. S. Jo, K. Y. Song, H. G. Park, S. Hwang, S. S. Al-Deyab, W. Y. Yoon, S. S. Yoon, ACS Appl. Mater. Interfaces 8 (2016) 9446-9453.

[10] M. Yu, D. Shao, F. Lu, X. Sun, H. Sun, T. Hu, G. Wang, S. Sawyer, H. Qiu and J. Lian, Electrochem. Commun. 34 (2013) 312-315.

[11] G. Zhang, S. Hou, H. Zhang, W. Zeng, F. Yan, C. C. Li and H. Duan, Adv. Mater. 27 (2015) 2400-2405.

[12] S. J. Yang, S. Nam, T. Kim, J. H. Im, H. Jung, J. H. Kang, S. Wi, B. Park and C. R. Park, J. Am. Chem. Soc. 135 (2013) 7394-7397.

[13] Shilpa, B. M. Basavaraja, S. B. Majumder and A. Sharma, J. Mater. Chem. A 3 (2015) 5344-5351.

[14] G.-L. Xu, Y. Li, T. Ma, Y. Ren, H.-H. Wang, L. Wang, J. Wen, D. Miller, K. Amine and Z. Chen, Nano Energy 18 (2015) 253-264.

[15] L. Hou, L. Lian, L. Zhang, G. Pang, C. Yuan and X. Zhang, Adv. Funct. Mater. 25 (2015) 238-246.

[16] Z. Li and L. Yin, J. Mater. Chem. A 3 (2015) 21569-21577.

Accepted manuscript

ACCEPTED MANUSCRIPT

[17] Z. Zhang, Z. Yang, R. Wang, Z. Feng, X. Xie and Q. Liao, Electrochim. Acta 134 (2014) 287-292.

[18] L. Gao, S. Li, D. Huang, Y. Shen and M. Wang, Electrochim. Acta 182 (2015) 529-536.

[19] H. Guo, T. Li, W. Chen, L. Liu, X. Yang, Y. Wang and Y. Guo, Nanoscale 6 (2014) 15168-15174.

[20] X. Ge, Z. Li, C. Wang and L. Yin, ACS Appl. Mater. Interfaces 7 (2015) 26633-26642.

[21] I. E. Collings, A. B. Cairns, A. L. Thompson, J. E. Parker, C. C. Tang, M. G. Tucker, J. Catafesta, C. Levelut, J. Haines, V. Dmitriev, P. Pattison and A. L. Goodwin, J. Am. Chem. Soc. 135 (2013) 7610-7620.

[22] H. Fan, J. Zheng, J. Hu, Y. Su, N. Zhao, J. Xu, F. Liu and F. Pan, Part. Part. Syst. Charact. 32 (2015) 771-778.

[23] Y. Zhou, X. Xu, B. Shan, Y. Wen, T. Jiang, J. Lu, S. Zhang, D. P. Wilkinson, J. Zhang and Y. Huang, Energy Storage Mater. 1 (2015) 103-111.

[24] H. S. Fan, H. Wang, N. Zhao, J. Xu and F. Pan, Sci. Rep. 4 (2014) 7426.

[25] H. Wang, Q. Pan, Y. Cheng, J. Zhao and G. Yin, Electrochim. Acta 54 (2009) 2851-2855.

[26] M.-S. Wu and H.-W. Chang, J. Phys. Chem. C 117 (2013) 2590-2599.

[27] Z. Zhou, K. Zhang, J. Liu, H. Peng and G. Li, J. Power Sources 285 (2015) 406-412.

[28] Y. Wang, X. Jiang, L. Yang, N. Jia and Y. Ding, ACS Appl. Mater. Interfaces 6 (2014) 1525-1532.

[29] H. Yu, X. Rui, H. Tan, J. Chen, X. Huang, C. Xu, W. Liu, D. Y. W. Yu, H. H. Hng, H. E. Hoster and Q. Yan, Nanoscale 5 (2013) 4937-4943.

[30] X. Sun, C. Zhou, M. Xie, H. Sun, T. Hu, F. Lu, S. M. Scott, S. M. George and J. Lian, J. Mater. Chem. A 2 (2014) 7319-7326.

[31] N. Li, S. X. Jin, Q. Y. Liao and C. X. Wang, ACS Appl. Mater. Interfaces 6 (2014) 20590-20596.

[32] C. Xiao, S. Zhang, S. Wang, Y. Xing, R. Lin, X. Wei and W. Wang, Electrochim. Acta 189 (2016) 245-251.

[33] M. Yu, A. Wang, Y. Wang, C. Li and G. Shi, Nanoscale 6 (2014) 11419-11424.

[34] F. Zou, X. Hu, Z. Li, L. Qie, C. Hu, R. Zeng, Y. Jiang and Y. Huang, Adv. Mater. 26 (2014) 6622-6628.

[35] G. Zhou, D.-W. Wang, F. Li, L. Zhang, N. Li, Z.-S. Wu, L. Wen, G. Q. Lu and H.-M. Cheng, Chem. Mater. 22 (2010) 5306-5313.

Accepted manuscript

Haosen Fan received his PhD from the Institute of Chemistry, Chinese Academy of Sciences (ICCAS) in 2012 under the supervision of Prof. Ning Zhao and Prof. Jian Xu. Currently he is a research fellow in Department of Materials Science & Engineering, Nanyang Technological University, Singapore. His current research interests focus on rational design of metal oxides, sulfides, selenides and carbides from coordination polymers for energy storage and conversion, including Li/Na ion batteries and electrocatalysts.

Hong Yu received her B. S. and Ph.D. from School of Materials Science and Engineering, Nanyang Technological University in 2011 and 2016, respectively. Currently, she is a research fellow at School of Materials Science and Engineering, Nanyang Technological University. Her research interests focus on the development and preparation of advanced nanomaterials for energy storage devices and electrocatalysis applications.

Yufei Zhang is currently an exchange PhD student under the supervision of Prof. Qingyu Yan in the School of Materials Science and Engineering at the Nanyang Technological University. She is now a PhD candidate under the supervision of Prof. Wei Huang and Prof. Xiaochen Dong cocultivated by Inner Mongolia University and Nanjing Tech. Her research focuses on the novel

Accepted manuscript

ACCEPTED MANUSCRIPT

synthesis of functional nanostructures materials for energy-related applications.

Jing Guo received his B. Sc majoring in chemistry from Peking University, China in 2013. He is now a PhD student at Laboratory of polymer Physics and Chemistry, Institute of Chemistry, the Chinese Academic of Science. His current research is focused on high performance biomimetic coating materials and polymer based carbon materials.

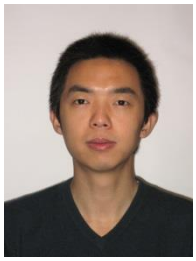

Zhen Wang is a postdoctoral scholar working at KTH Royal Institute of Technology, Sweden. He received his B.S in polymer materials and engineering from Dalian University of Technology, China, in 2009. His M.S. in materials engineering and Ph.D. in polymer chemistry and physics were both obtained from Institute of Chemistry, Chinese Academy of Sciences, China, in 2012 and 2015 respectively. His research interests are focused on porous materials and their applications in energy storage devices.

Hao Wang is a lecturer at Department of Environmental Engineering, North China institute of Science & Technology, China. He received his B.Eng. in Chemistry and Chemical Engineering Department of Hefei University of Technology, China in 2007 and Ph.D. from Institute of Chemistry Chinese Academy of Sciences in 2015. His research interests focused on conducting polymer materials and biomimetic materials for electrochromic devices, electrode materials and

Accepted manuscript

flameresistant application.

Ning Zhao is a Professor at the Institute of Chemistry, Chinese Academy of Sciences (ICCAS). He received his B.S. from Tianjin University, China in 2000 and Ph.D. from ICCAS in 2006. After one year postdoctoral research in University of Montreal, he returned to ICCAS and promoted to a full professor in 2014. His research interest includes biomimetic materials, functional surfaces and porous materials.

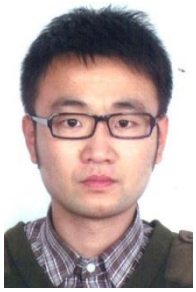

Hongbo Geng is currently an exchange student under the supervision of Prof. Qingyu Yan in the S chool of Materials Science and Engineering at the Nanyang Technological University. He received his M.S. degree from Soochow University of China in 2014. His research interests cover design an d synthesis of functional nanostructures and composite materials for energy-related applications su ch as electrocatalysis, batteries, and hydrogen storage.

Zhengfei Dai received his PhD from the Institute of Solid State of Physics, CAS, in 2013 under the supervision of Prof. Weiping Cai. Then, he worked at Department of Materials Science & Engineering, Korea University, South Korea. Since Dec., 2014, he has worked at Department of Chemistry, Kyoto University, Japan as a JSPS research fellow. From Feb. 2016, he has worked as

Accepted manuscript

ACCEPTED MANUSCRIPT

a research fellow in Department of Materials Science & Engineering, Nanyang Technological University, Singapore. His current research interests focus on gas sensors, secondary battery, and electrocatalysts.

Qingyu Yan is an associate professor at School of Materials Science and Engineering, Nanyang Technological University, Singapore. He received his B.Sc. in Materials Science and Engineering from Nanjing University, China in 1999 and Ph.D. from Materials Science and Engineering Department of State University of New York at Stony Brook in 2004. He then joined the Materials Science and Engineering Department of Rensselaer Polytechnic Institute as a postdoctoral researcher before joining Nanyang Technological University in 2007. His research interests focused on nanostructured materials and their integration/assembly for electrode materials for energy storage devices, thermoelectric module, magnetic devices and photovoltaic module applications.

Jian Xu is a Professor at the Institute of Chemistry, Chinese Academy of Sciences (ICCAS). He received his B.S. and M.S. from Chengdu University of Science and Technology from 1982 and 1985, respectively, and Ph.D. from Sichuan University in 1994. He joined ICCAS in 1995, first as a postdoctoral researcher for two years and then a full professor in 1999. His research interest focuses on high performance fibers and functional materials.

Accepted manuscript

ACCEPTED MANUSCRIPT

Highlights

- Hierarchical yolk shell structures assembled from ZnO@C nanocrystals were successfully prepared from zinc-cyanide hybrid coordination polymers.
- The micro-nano secondary structure can both achieve high packing density and facilitate the Li^+ ion diffusion.
- The carbon coated ZnO nanocrystals provide high conductivity and confine ZnO nanocrystals expansion.
- The yolk-shell structure exhibit ultra-stable cycle life because it can further buffer the strain during repeated cycling to maintain the structural integrity.

Accepted manuscript